JACS
JOURNAL OF THE AMERICAN CHEMICAL SOCIETY
Article
Cite This: J. Am. Chem. Soc. 2019, 141, 14220−14229
pubs.acs.org/JACS

Depolymerization of Bottlebrush Polypentenamers and Their Macromolecular Metamorphosis

William J. Neary, Taylor A. Isais, and Justin G. Kennemur*

Department of Chemistry and Biochemistry, Florida State University, Tallahassee, Florida 32306, United States

Supporting Information

ABSTRACT: The depolymerization of bottlebrush (BB) polymers with varying lengths of polycyclopentene (PCP) backbone and polystyrene (PS) grafts is investigated. In all cases, ring closing metathesis (RCM) depolymerization of the PCP BB backbone appears to occur through an end-to-end depolymerization mechanism as evidenced by size exclusion chromatography. Investigation on the RCM depolymerization of linear PCP reveals a more random chain degradation process. Quantitative depolymerization occurs under thermodynamic conditions (higher temperature and dilution) that drives RCM into cyclopentenes (CPs), each bearing one of the original PS grafts from the BB. Catalyst screening reveals Grubbs' third (G3) and second (G2) generation catalyst depolymerize BBs significantly faster than Grubbs' first generation (G1) and Hoveyda−Grubbs' second generation (HG2) catalyst under identical conditions while solvent (toluene versus $CHCl_3$) plays a less significant role. The length of the BB backbone and PS side chains also play a minor role in depolymerization kinetics, which is discussed. The ability to completely deconstruct these BB architectures into linear grafts provides definitive insights toward the ATRP "grafting-from" mechanism originally used to construct the BBs. Core−shell BB block copolymers (BBCPs) are shown to quantitatively depolymerize into linear diblock polymer grafts. Finally, the complete depolymerization of BBs into α-cyclopentenyl-PS allows further transformation to other architectures, such as 3-arm stars, through thiol−ene coupling onto the CP end group. These unique materials open the door to stimuli-responsive reassembly of BBs and BBCPs into new morphologies driven by macromolecular metamorphosis.

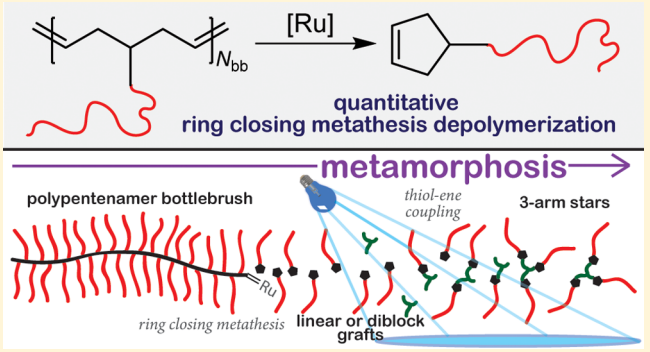

INTRODUCTION

Self-immolative polymers (SIPs)[1−5] are a subset of end-to-end depolymerizable polymers and stimuli-responsive materials[6] gaining considerable attention for a variety of potential applications including signal amplification,[7−9] cargo delivery/release,[10−17] protein labeling,[18] antimicrobials,[19,20] microfluidic pumps,[21] and recyclable materials.[22] Unlike traditional degradation of polymers, which occurs through random chain cleavage events, an end-to-end depolymerization occurs through an unzipping process that is often triggered by an external stimulus.[1−5] These materials are typically prepared through the end-capping of a polymer chain with a specific chemistry that stabilizes the polymer under ambient conditions. The term "self-immolative" suggests self-sacrifice following an external stimulus, which can be irradiative, thermal, or chemical, and has been successfully shown to trigger the depolymerization event on a variety of end-groups and backbone chemistries to date.[7−37] While many SIPs have been limited to linear and dendritic based topologies, a few have expanded to more complex architectures, such as grafted polymers.[7,32,38] Recently, the first bottlebrush (BB) SIP was reported by Zhang et al.[39] which consists of a poly(benzyl ether) backbone with alkyne pendants and an end group with a *tert*-butyldimethylsiloxy (TBDMS) or allyl chloroformate (ACF) capping. Azide terminated poly(ethylene glycol) (PEG) or polystyrene (PS) side chains (2−4 kg mol^{-1}) were "grafted-to" the alkyne backbone pendants to produce the BBs. Upon the addition of tetrabutylammonium fluoride (TBAF) or Pd(0), uncapping of TBDMS or ACF end groups, respectively, promoted backbone unzipping. While this work was the first example of an end-to-end depolymerization of a BB, full depolymerization of these materials was shown to be hampered by rigid side chains (PS) which are proposed to limit optimal backbone conformation for unzipping.[39]

Polycyclopentenes (PCP)s, also termed polypentenamers, are derived from ring-opening metathesis polymerization (ROMP) of cyclopentene (CP) and are a unique class of elastomers that can depolymerize through ring-closing metathesis (RCM) to reform their low strain CP monomers.[40] While their ability to depolymerize was first determined in 1972,[41] these materials have remained largely underutilized due to long-standing challenges in synthesizing these polymers.[40] Unlike highly strained cycloalkene derivatives,

Received: May 23, 2019
Published: August 12, 2019

DOI: 10.1021/jacs.9b05560
J. Am. Chem. Soc. 2019, 141, 14220−14229

which are the typical monomers of choice for ROMP, the low ring strain of CP significantly reduces the ceiling temperature (T_c) and results in a polymerization−depolymerization equilibrium that is highly sensitized to reaction temperature and monomer concentration.[40] Recent reports have begun to rekindle interest in utilizing the low T_c of polypentenamers advantageously. Tuba et al. showed that silicon-functionalized polypentenamers could be depolymerized quantitatively, leading to their possible use in recyclable tires.[42] Liu et al. utilized the dynamic equilibrium of multifunctional polypentenamers to produce covalently adaptable networks (CANs) that assemble and disassemble at low and high temperature, respectively.[43]

Badamshina et al. produced the only discovered report that investigates the mechanism of PCP depolymerization, and it was determined that degradation occurs randomly through metathesis events along the polymer chains.[44] The catalyst, in this case tungsten,[44] coordinates at one of many accessible internal olefins of PCP and cleaves it into two smaller chains; one bears the active catalyst, and the other is stable. The active chain then rapidly unzips through RCM, generating a CP monomer and eventually a new active catalyst methylidene species. The new catalyst can subsequently coordinate to other chains, repeating the process until quantitative depolymerization has been achieved.[44] This degradation is not an end-to-end depolymerization but rather mirrors the depolymerization process (i.e., random chain cleavage) of most polymers.

We envisioned that a BB polymer with a backbone comprised of a polypentenamer may also depolymerize quantitatively to produce linear grafts with a CP end group functionality. Herein we explore this hypothesis and discover that the depolymerization of the BB architecture appears to occur in an end-to-end fashion, releasing linear grafts quantitatively under thermodynamically favorable conditions. Investigations on the effects of side chain degree of polymerization (N_{sc}), backbone degree of polymerization (N_{bb}), and catalyst activity are discussed. Although the deconstruction of the BBs provides definitive insight on the original BB material, we have elevated these investigations to provide evidence for the complete deconstruction and facile metamorphosis of complex BBs into new macromolecular architectures for the first time.

RESULTS AND DISCUSSION

We recently reported the ability to polymerize CP and derivatives with suitable ring strain to high conversion, targeted molar mass, and low dispersity ($Đ$) through a method we termed variable temperature ROMP (VT-ROMP).[45] Soon after, we extended the VT-ROMP method to a CP monomer functionalized with a bromoisobutyryl group (CPBIB), allowing the synthesis of well-defined macroinitiators suitable for "grafting-from" by atom transfer radical polymerization (ATRP) (Scheme 1).[46] The resulting materials introduced a new type of BB system consisting of a polypentenamer backbone and a variety of possible graft chemistries; in the case of Scheme 1, polystyrene (PS) is used. Characterization of these BBs concluded a high degree of control over N_{bb} and N_{sc} in addition to near-quantitative grafting efficiency and low $Đ$.[46]

Full Depolymerization and Insight on the Grafting-from Technique. Full depolymerization of the polypentenamer backbone would allow additional insight into the "grafting-from" methodology to confirm the number-average molar mass (M_n) and $Đ$ of the grafts. To explore this, we first

Scheme 1. Synthesis[46] and Depolymerization of Bottlebrush Polypentenamers

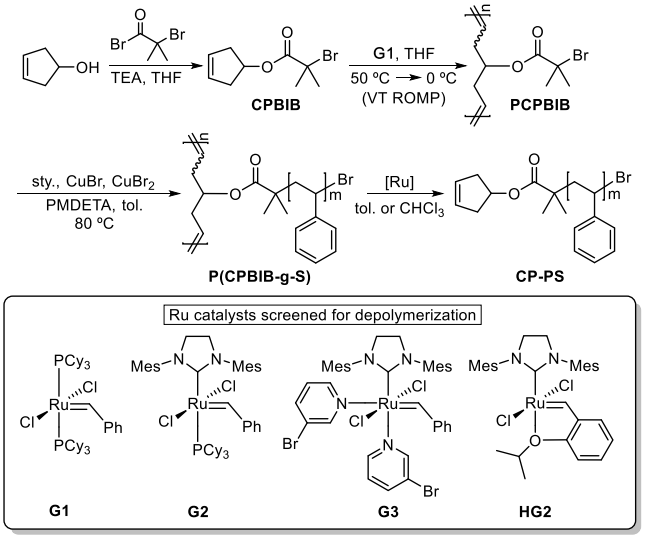

synthesized four new BB samples (Table 1), using our previously reported strategy[46] as outlined in Scheme 1. Subscript numbers within the BB sample IDs in Table 1 represent N_{bb} and N_{sc}, respectively. Prior to grafting-from, PCPBIB macroinitiators were characterized through size exclusion chromatography (SEC) to determine N_{bb} (Figures S1 and S3) and their microstructures were also confirmed through ^{1}H NMR spectroscopy (Figures S2 and S4). It is worth noting that P(CPBIB$_{181}$) has the largest N_{bb} (181) reported to date for these systems and the ability to achieve such high molar mass is largely due to an extensive triple distillation method to remove linear olefin contaminants from the monomer.[47] After ATRP of styrene (S), comparative integration of the backbone olefin signals with the aryl proton signals of the PS graft repeating units by ^{1}H NMR provides N_{sc} (Figures S5−S8). Integration of the end group signals at ∼4.5 ppm, which represent an overlap of the backbone methine proton and the ω-bromo-methine proton at the end of the PS grafts, are also in excellent agreement with the N_{sc} analysis (Figures S5−S8).

For initial depolymerization studies, P(CPBIB$_{181}$-g-S$_{18}$) and P(CPBIB$_{97}$-g-S$_{18}$) were chosen since these BBs have identical N_{sc}, yet the former has a backbone that is nearly double in length. Both BBs were subjected to depolymerization in toluene (5% w/v BB) at 70 °C for 24 h using Hoveyda−Grubbs' second generation catalyst (HG2, Scheme 1) at a concentration of 10 mol % relative to the initial concentration of olefins, [olefin]$_0$. Figure 1 displays the SEC traces of the BBs before and after depolymerization while Table 1 displays numerical characterization values. As seen in Figure 1, quantitative depolymerization of both BBs (solid traces) into narrow PS grafts (dash-dot traces) has occurred under these conditions. More specifically, the α-cyclopentenyl-PS products, CP-PS$_{21}$ and CP-PS$_{20}$, produced from depolymerization of P(CPBIB$_{181}$-g-S$_{18}$) and P(CPBIB$_{97}$-g-S$_{18}$), respectively, have nearly identical elution times and both products have a monomodal refractive index (RI) signal and narrow $Đ$ (1.10 ± 0.06). A complete depolymerization of P(CPBIB$_{97}$-g-S$_{44}$) and P(CPBIB$_{181}$-g-S$_{28}$) was also successful under similar conditions, producing CP-PS$_{43}$ (M_n = 4.6 kg mol^{-1}, $Đ$ = 1.12) and CP-PS$_{27}$ (M_n = 3.2 kg mol^{-1}, $Đ$ = 1.02), respectively (Figures

DOI: 10.1021/jacs.9b05560
J. Am. Chem. Soc. 2019, 141, 14220−14229

Table 1. Characterization Data for Synthesized Bottlebrushes and Their Grafts Following Quantitative Depolymerization[a]

BB ID	N_{sc}[b]	N_{bb}[c]	$Đ$[c]	Graft ID	$N_{PS,SEC}$[c]	$N_{PS,NMR}$[b]	$Đ$[c]
P(CPBIB$_{97}$-*g*-S$_{18}$)	18	97	1.18	CP-PS$_{20}$	18	20	1.16
P(CPBIB$_{97}$-*g*-S$_{44}$)	44	97	1.27	CP-PS$_{43}$	44	43	1.12
P(CPBIB$_{181}$-*g*-S$_{18}$)	18	181	1.35	CP-PS$_{21}$	20	21	1.05
P(CPBIB$_{181}$-*g*-S$_{28}$)	28	181	1.35	CP-PS$_{27}$	31	27	1.02

[a]All depolymerizations were conducted at 10 mol % HG2 relative to [olefin]$_0$ and a BB dilution of 5% (w/v) in toluene at 70 °C for 24 h. [b]Determined by ^{1}H NMR analysis (CDCl$_3$, 25 °C). [c]Determined by SEC-MALS.

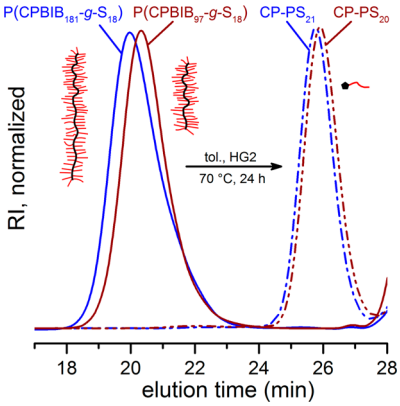

Figure 1. SEC traces of bottlebrushes P(CPBIB$_{181}$-*g*-S$_{18}$) (blue solid trace, M_n = 248.6 kg mol^{-1}, $Đ$ = 1.35) and P(CPBIB$_{97}$-*g*-S$_{18}$) (red solid trace, M_n = 231.1 kg mol^{-1}, $Đ$ = 1.18) and their quantitative depolymerization to α-cyclopentenyl polystyrene grafts CP-PS$_{21}$ (blue dash-dot trace, M_n = 2.1 kg mol^{-1}, $Đ$ = 1.05) and CP-PS$_{20}$ (red dash-dot trace, M_n = 1.9 kg mol^{-1}, $Đ$ = 1.16), respectively. Both depolymerizations were performed in toluene ([olefin]$_0$ = 24 mM (5% (w/v)), [cat.]$_0$ = 2.4 mM) at 70 °C for 24 h using HG2 catalyst.

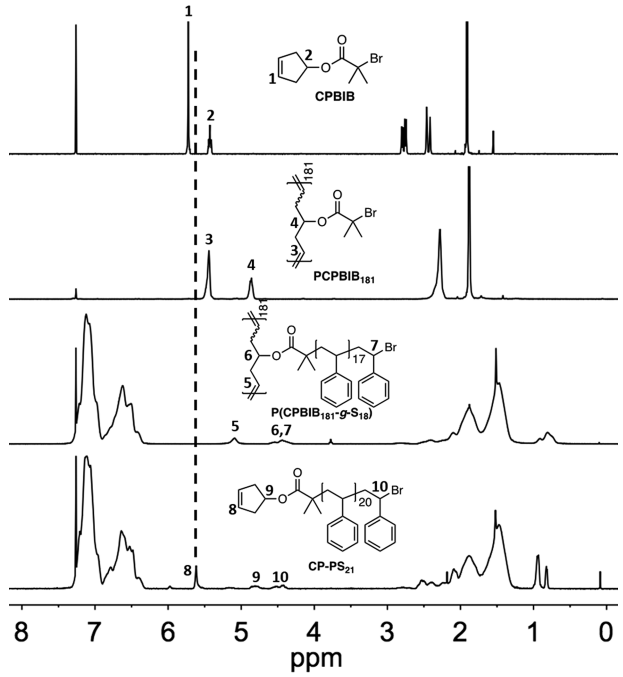

Figure 2. Stacked ^{1}H NMR spectra (CDCl$_3$, 25 °C) of CPBIB monomer (top), PCPBIB$_{181}$ macroinitiator (second from top), P(CPBIB$_{181}$-*g*-S$_{18}$) bottlebrush (second from bottom), and the CP-PS$_{21}$ grafts (bottom) following backbone depolymerization. Each transformation has unique olefin and methine proton signals that are annotated numerically in the spectra and further visually guided by the dashed line.

S9 and S10). Figure 2 displays stacked ^{1}H NMR (25 °C, CDCl$_3$) spectra illustrating the changes in chemical shifts associated with the protons of CPBIB monomer, PCPBIB$_{181}$ macroinitiator, the P(CPBIB$_{181}$-*g*-S$_{18}$) BB, and CP-PS$_{21}$ grafts after depolymerization. As guided visually by the dashed line, each transformation produces unique chemical shifts associated with the olefin proton signals. The α-cyclopentenyl olefin proton signal (5.67 ppm, annotated as 8) of the CP-PS products were comparatively integrated to the aryl protons of the PS repeating units to determine $N_{PS,NMR}$ for each sample in Table 1 (Figures S11, S16, S21, and S26). Subscript numbers of the CP-PS graft IDs in Table 1 represent the number-average degree of polymerization determined by ^{1}H NMR. Differential scanning calorimetry (DSC) analysis of each CP-PS sample is also consistent with the transformation to linear PS. The P(CPBIB-*g*-S) BBs have been previously shown to reach a glass transition temperature (T_g) of >90 °C with only an $N_{sc} \approx 18$.[46] Once the BBs are depolymerized into linear grafts, the CP-PS$_{20}$, CP-PS$_{21}$, CP-PS$_{27}$, and CP-PS$_{43}$ samples adopt a midpoint T_g of 75, 77, 85, and 90 ± 3 °C, respectively (Figures S14, S19, S24, and S29).

The ability to quantitatively depolymerize the BB backbone permits insight into the molecular properties of the grafts that are not possible while the material exists in the BB state. Although ATRP is now a well-established technique that is known to provide a high degree of control over the solution polymerization of S,[48] questions may still arise regarding uniformity and chain end fidelity when the grafts are grown within a densely populated space, such as the backbone of a BB system. The SEC traces of the depolymerized BBs and the data in Table 1 allow for the following conclusions. The narrow $Đ$ (1.02−1.16) of all CP-PS samples indicate that control is maintained and that all of the grafts are successfully polymerized in a unified fashion. Additionally, N_{sc} determined by ^{1}H NMR characterization of the intact BB assumes that every PCP repeating unit successfully produced a graft. Disparity between N_{sc} and N_{PS} after depolymerization is a good indication of nonquantitative grafting efficiency. When N_{sc} to $N_{PS,SEC}$ and $N_{PS,NMR}$ in Table 1 are compared, they are in excellent agreement. This supports our prior claim, based on ^{13}C NMR analysis of the BB, that grafting efficiency is near-quantitative.[46] Lastly, the ω-bromo-methine proton signals (annotated as 10 in Figure 2) were also comparatively integrated (Figures S11, S16, S21, and S26) and are in excellent agreement with the CP end group analysis indicating high fidelity of the bromine end group throughout the grafting-from, workup, and depolymerization process. The latter is important to note since Ru-based catalysts have been shown to have activity for ATRP.[49]

Ru Catalyst Effects and Evidence of End-to-End Depolymerization. To monitor and gain further mechanistic insight into BB depolymerization, a series of experiments were

DOI: 10.1021/jacs.9b05560
J. Am. Chem. Soc. 2019, 141, 14220−14229

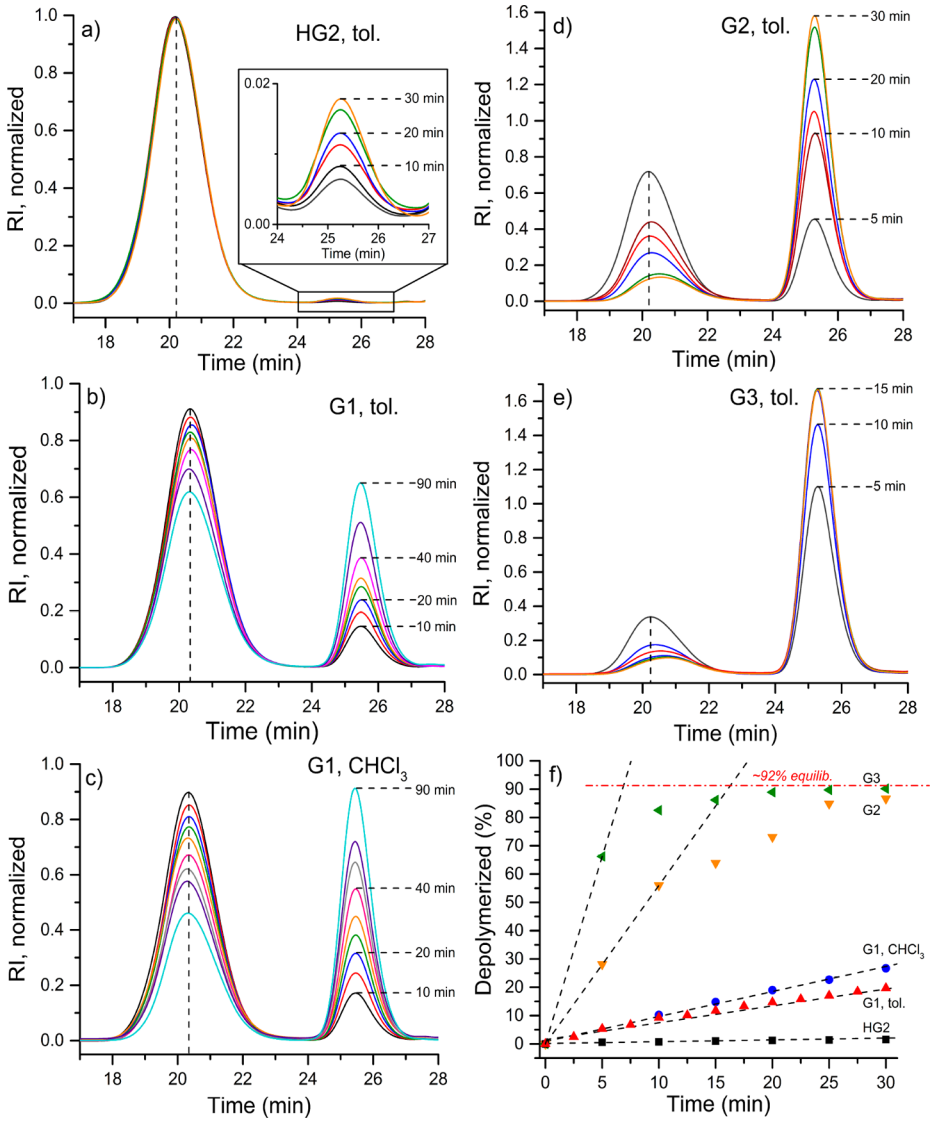

Figure 3. Normalized SEC traces over time during depolymerization of P(CPBIB$_{97}$-*g*-S$_{44}$) using (a) HG2 in toluene, (b) G1 in toluene, (c) G1 in $CHCl_3$, (d) G2 in toluene, and (e) G3 in toluene. Each depolymerization was performed at 25 °C using $[olefin]_0$ = 10 mM and $[cat.]_0$ = 0.5 mM. Varying timestamps are annotated in each plot as a guide to the eye. Plot (f) displays kinetic analysis of depolymerization as a function of time for each study (a–e) and reveals an equilibrium at ~92% depolymerization under these conditions.

performed on P(CPBIB$_{97}$-*g*-S$_{44}$), $[olefin]_0$ = 10 mM, at 25 °C in toluene using a variety of readily available Ru catalysts, $[cat.]_0$ = 0.5 mM (5 mol %), displayed in Scheme 1. Aliquots were taken at known time intervals and immediately quenched in a large excess of ethyl vinyl ether to deactivate the catalyst. Figure 3 displays the resulting SEC traces of the terminated aliquots at varying depolymerization times using Grubbs' first generation (G1), second generation (G2), third generation (G3), and HG2 catalyst at time intervals up to 90 min. For information about solvent effects, G1 was also investigated in $CHCl_3$, a medium polarity solvent, under identical conditions (Figure 3c). The SEC traces in Figure 3 are normalized by the overall integration ratios to provide clarity. The specific integration ratios of each RI signal for the BB and the CP-PS peaks allow for determination of the % depolymerization of the BBs and are plotted as a function of time for each experiment in Figure 3f.

As discussed, CP has a low ring strain ($-\Delta H_p$ = 23.4 kJ mol^{-1})[50] which promotes a low T_c (32 ± 3 °C at 1 M) and allows RCM of PCP to occur readily under conditions that thermodynamically favor depolymerization (i.e., diluted and/or higher temperatures).[40] Tuba et al. reported that linear PCP will completely depolymerize within 4 min at ambient temperatures at a dilution of 5 w/v% PCP in toluene using HG2 catalyst (0.4 mol %).[42] While the exact mechanism for the depolymerization was undetermined, previous literature[44] suggests that it occurs through random chain cleavage of internal olefins within the PCP backbone as shown on the left side of Scheme 2. When depolymerization occurs in this manner, a gradual reduction and broadening of the molar mass distribution occurs over time (due to the production of smaller dormant chains) until quantitative depolymerization has occurred.[44] Using SEC and ^{1}H NMR, we monitored the depolymerization of a linear PCP sample (M_n = 30.7 kg mol^{-1}, $Đ$ = 1.2) with G1 in $CDCl_3$ at 25 °C over the course of 4 min (Figures S31 and S32). Indeed, when compared to the BB system in Figure 3c and 3f, PCP depolymerized much faster with ~85% PCP depolymerization in 4 min. While ^{1}H NMR

DOI: 10.1021/jacs.9b05560
J. Am. Chem. Soc. 2019, 141, 14220–14229

Scheme 2. Depolymerization Outcomes Depending on the Type of Initial Olefin Coordination (Internal versus Terminal) for HG2 or G2 Catalyst on a Polypentenamer Backbone

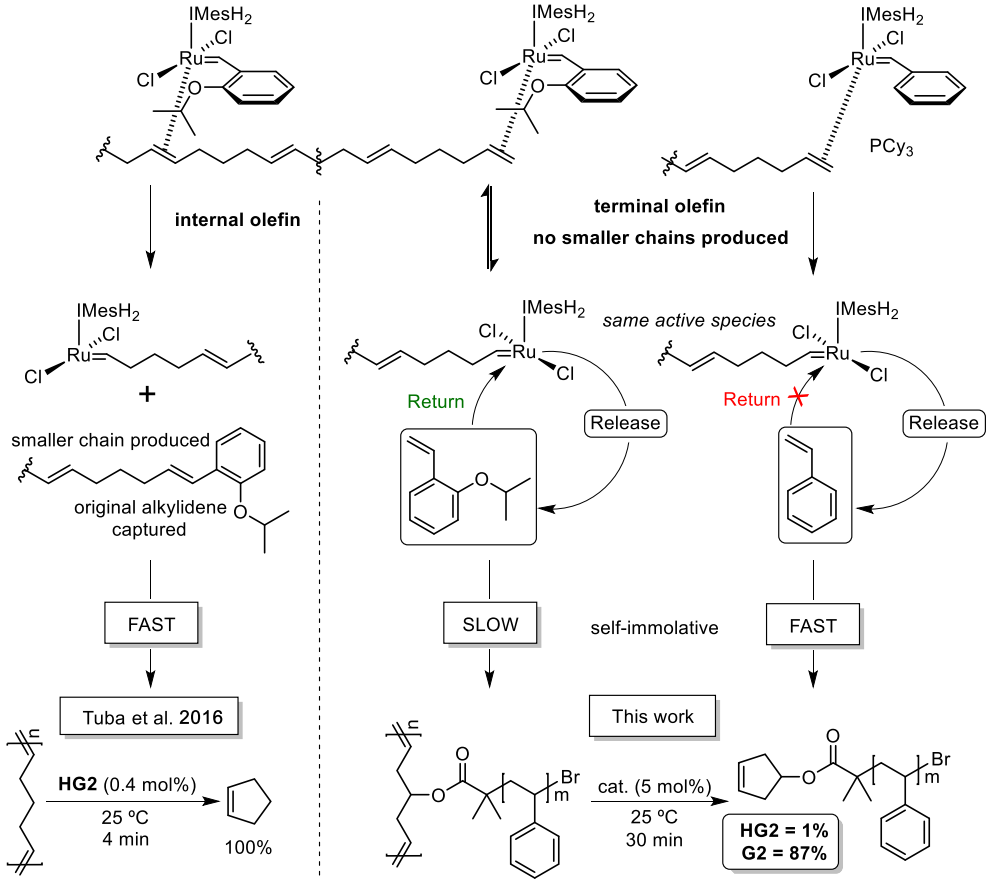

confirms the disappearance of the PCP olefin proton signals and the appearance of CP olefin signals over time, SEC analysis displays a gradual reduction in PCP molar mass and slight broadening of the RI signal. Combined, these indicate that PCP depolymerization is likely occurring through random metathesis events along the chain. The ring strain of CPBIB, $-\Delta H_p$ = 22.6 kJ mol^{-1},[46] is less than CP and therefore has a slightly higher propensity to undergo RCM under similar conditions ($T_c \approx 30$ °C at 1 M).[40] When observing the depolymerization of our BBs under similar dilution (5% w/v), solvent, and temperature (25 °C) in addition to using HG2 (5 mol %), only 1% of P(CPBIB$_{97}$-*g*-S$_{44}$) depolymerized after 30 min (Figure 3a,f).

Depolymerization of P(CPBIB$_{97}$-*g*-S$_{44}$) under identical conditions was performed using G1, G2, and G3 to gain insight into the effect that the catalyst has on the rate of depolymerization. Interestingly, G1 showed a >10-fold increase in depolymerization rate versus HG2 even though G1 is generally accepted as less active for RCM (Figure 3b). With G2 (Figure 3d) and G3 (Figure 3e), an even more rapid depolymerization occurred with a >100- and >300-fold rate increase versus HG2, respectively. Although depolymerization is fast at 25 °C using G2 and G3, both reached an equilibrium around 92% depolymerization after 30 min (Figure 3f). As shown in Figure S9, complete depolymerization of P(CPBIB$_{97}$-*g*-S$_{44}$) can be achieved at higher temperature. The fact that an equilibrium can be seen and adjusted with temperature and/or concentration is exciting and suggests that reversibility of the depolymerization−repolymerization of the BB is possible; however, it will not be the focus of this work. An additional experiment was conducted with $CHCl_3$ and G1 (Figure 3c) which displayed a slight increase in the rate of depolymerization versus toluene (Figure 3f) but was still much slower than PCP using G1 in $CDCl_3$ (Figure S31). Hence, solvent effects appear minor compared to the choice of catalyst for BB depolymerization kinetics.

One of the most notable observations for each BB depolymerization, regardless of catalyst choice, is that no polymer is observed by SEC at elution times in-between the extremities of the original BB and CP-PS peaks. The absence of chains with molar masses at intermediate values suggests that internal olefin coordination and chain cleavage is not occurring (Scheme 2, left side) and that depolymerization is likely occurring in an end-to-end fashion through initial catalyst coordination with the terminal olefin on one end of the BB (Scheme 2, right side) followed by complete RCM of the BB to the other chain end and installation of a phenyl alkylidene onto the Ru catalyst. We believe this to be the most plausible explanation for these observations currently. For depolymerizations using G2 and G3, a slight shifting of the BB peak is observed once the depolymerization approaches equilibrium (Figure S33) even though dispersity remains consistent and we believe this to be an artifact of the reversible polymerization−depolymerization mechanism occurring at this stage.

The depolymerization of the BBs can also be monitored by ^{1}H NMR by observing the loss of PCP olefin signal and the increase in CP olefin signal over time. To illustrate this, we performed a depolymerization on P(CPBIB$_{97}$-*g*-S$_{18}$) in $CDCl_3$

DOI: 10.1021/jacs.9b05560
J. Am. Chem. Soc. 2019, 141, 14220−14229

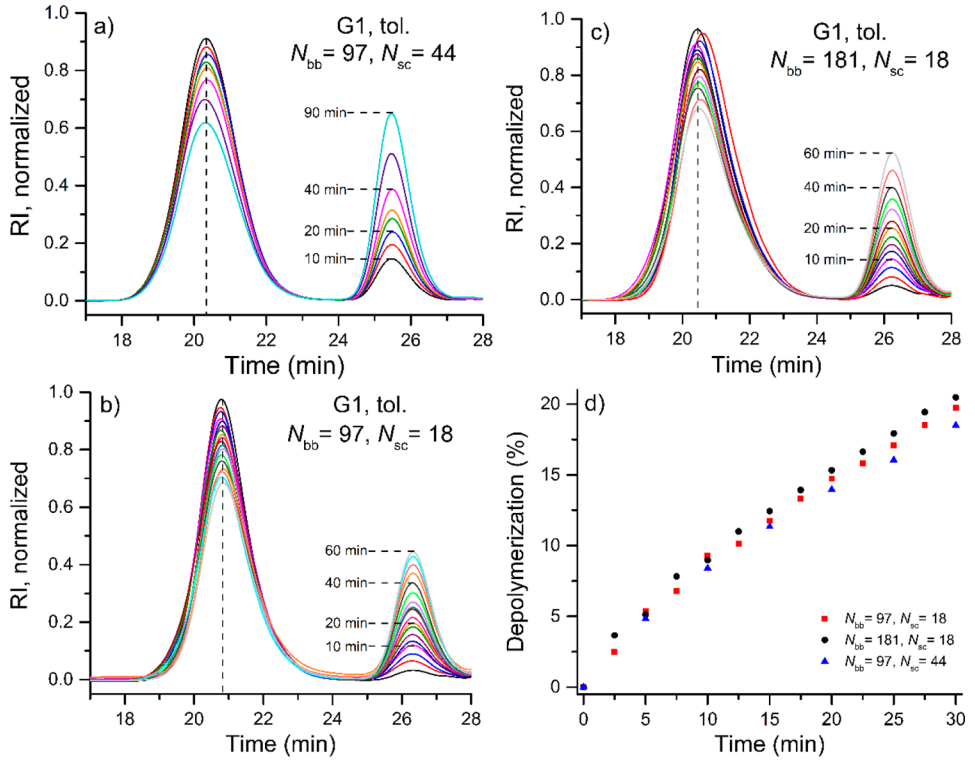

Figure 4. Normalized SEC traces over time during depolymerization of (a) P(CPBIB$_{97}$-*g*-S$_{44}$), (b) P(CPBIB$_{97}$-*g*-S$_{18}$), and (c) P(CPBIB$_{181}$-*g*-S$_{18}$) using G1 in toluene at 25 °C; $[\text{olefin}]_0$ = 10 mM and $[\text{cat.}]_0$ = 0.5 mM. Varying timestamps are annotated in each plot as a guide to the eye. Plot (d) displays depolymerization as a function of time for each study (a–c) showing minor effects of brush length and backbone length on depolymerization kinetics under these conditions.

($[\text{olefin}]_0$ = 24 mM, $[\text{G1}]_0$ = 1.2 mM) at 25 °C and monitored the depolymerization at known timestamps (Figure S34 and Table S1). The rate of depolymerization appears slightly faster under these conditions versus Figure 3c, likely due to the slightly increased $[\text{olefin}]_0$. Table S1 also illustrates that the *ω*-bromo-methine signal integration remains relatively constant throughout the depolymerization while the CP olefin signal increases and the PCP olefin signal decreases, as expected. While ^{1}H NMR provides this information, it does not provide insight on how the molar mass and *Đ* of the BB are changing with time whereas SEC allows observation of the relative kinetics and mechanism simultaneously.

Another Case for the Boomerang Mechanism? While HG2 appears to be a highly effective catalyst for RCM of linear PCP at 25 °C,[42] it is a surprisingly poor choice for the depolymerization of the BBs. One possible explanation for the significantly reduced depolymerization rate of HG2 is the long-debated release–return or boomerang mechanism that recently received compelling evidence by Fogg and co-workers.[51] In the specific case where HG2 first binds to a terminal olefin, such as the proposed end-to-end depolymerization mechanism, the release of *o*-isopropoxystyrene occurs and the catalyst achieves an active 14 e^- state that is indiscernible from G2 in the active state (Scheme 2 middle, right). The reuptake (return) of *o*-isopropoxystyrene to the active Ru species detaches it from the chain end and produces the original HG2 catalyst-free in solution, thereby impeding a rapid unzipping event. This release–return mechanism has been shown to be a highly competitive process, effectively occurring even within a large excess of substrate and allows for extremely low HG2 catalyst loadings for metathesis reactions.[51] In our case, the release of HG2 back into the depolymerization solution and the potential difficulties associated with the catalyst returning to find the terminal chain end could be a viable reason for the greatly reduced kinetics of HG2. To further test this hypothesis we performed a depolymerization on P(CPBIB$_{181}$-*g*-S$_{18}$) using HG2 at higher temperature (70 °C) to increase the depolymerization rate and allow for the observation of how the BB molar mass changes over time by SEC (Figure S35 and Table S2). We observed a gradual increase of the BB peak elution time (shifting to lower molar mass) during the course of depolymerization with only a slight increase to the peak's dispersity (∼1.3–1.4). Although this experiment helps support our hypothesis that HG2 is gradually depolymerizing the BBs through the release–return mechanism, it cannot be ruled out that cross-metathesis is absent at such elevated temperatures due to the slight increase in *Đ*.

Effect of Graft and Backbone Length on Depolymerization. To determine the effect of N_{sc} and N_{bb} on the depolymerization kinetics, another series of experiments were performed using G1 in toluene, $[\text{olefin}]_0$ = 10 mM and $[\text{cat.}]_0$ = 0.5 mM), on P(CPBIB$_{97}$-*g*-S$_{44}$), P(CPBIB$_{97}$-*g*-S$_{18}$), and P(CPBIB$_{181}$-*g*-S$_{18}$) and monitored at known time intervals by SEC for up to 90 min (Figure 4). Here again the rate of depolymerization can be monitored by comparative integration of the BB and CP-PS RI signals and is provided for the initial 30 min of depolymerization in Figure 4d.

Two BBs, P(CPBIB$_{97}$-*g*-S$_{44}$) and P(CPBIB$_{97}$-*g*-S$_{18}$), with identical N_{bb} and different N_{sc} were depolymerized separately under the same conditions and at the same concentration of polymer chains (0.1 *μ*M) (Figure 4a and 4b, respectively). In other words, these solutions have the same concentration of terminal olefins and any difference associated with depolymerization can be attributed to the length of the grafts. As seen in

DOI: 10.1021/jacs.9b05560
J. Am. Chem. Soc. 2019, 141, 14220–14229

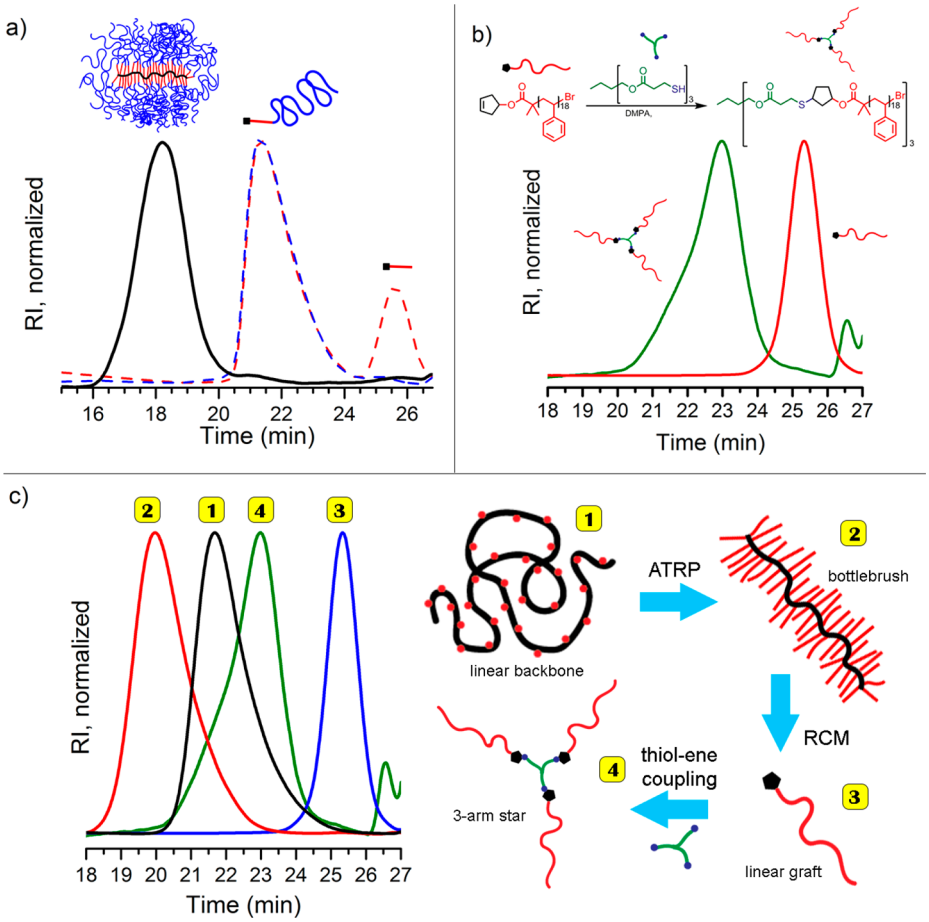

Figure 5. Examples of macromolecular metamorphosis. (a) Normalized SEC traces displaying the depolymerization of previously synthesized P(CPBIB$_{82}$-*g*-(S$_{21}$-*b*-MMA$_{100}$)) (black trace) to produce linear PS-*b*-PMMA diblock polymer (M_n = 39.7 kg mol^{-1}, $Đ$ = 1.14) and PS homopolymer (red trace). The latter provides insight on the number of PS grafts that did not successfully initiate an MMA block. Soxhlet extraction to remove the PS grafts produced only the diblock polymer (blue trace). (b) Normalized SEC traces of CP-PS$_{21}$ produced from depolymerization of a P(CPBIB$_{181}$-*g*-S$_{18}$) (red trace) and their transformation into a 3-arm star, TMP-(PS$_{21}$)$_3$, (green trace) following photoinitiated thiol−ene coupling with trimethylolpropane tris(3-mercaptopropionate) and DMPA photoinitiator. (c) An overall cartoon rendition and normalized SEC traces of the varying forms of architectural metamorphosis possible from [1] a linear PCPBIB$_{181}$ backbone (black trace) to [2] P(CPBIB$_{181}$-*g*-S$_{18}$) bottlebrush (red trace) to [3] linear CP-PS$_{21}$ grafts (blue trace) to [4] 3-arm stars (TMP-(PS$_{21}$)$_3$) (green trace).

Figure 4d, these two BBs depolymerized at very similar rates (blue triangles versus red squares, respectively), although P(CPBIB$_{97}$-*g*-S$_{44}$) does appear a little slower after 30 min.

Comparison of the depolymerization rates between P(CPBIB$_{97}$-*g*-S$_{18}$) and P(CPBIB$_{181}$-*g*-S$_{18}$) were performed at identical olefin and catalyst concentrations ([olefin]$_0$ = 10 mM, [cat.] = 0.5 mM). The fact that P(CPBIB$_{97}$-*g*-S$_{18}$) has a backbone nearly half the length of P(CPBIB$_{181}$-*g*-S$_{18}$) means that the initial concentration of terminal olefins (i.e., polymer chains) is 0.10 μM and 0.06 μM, respectively. Our initial hypothesis was that the rate would be controlled by the catalyst finding a terminal olefin on the BB system, and it was expected that the rate of depolymerization is first order with regards to the concentration of terminal olefins. However, the depolymerization rates of these experiments were again very similar (Figure 4d, red squares and black circles). This suggests that the depolymerization rate is zero order with respect to terminal olefins, a particularly intriguing result. While G1 has been shown to have an initiation rate that is dependent on olefin concentration, the rate of PCy$_3$ dissociation/reassociation over olefin metathesis is extremely high.[52] Therefore, the governing kinetics of these depolymerizations, specifically for G1, may be independent of initiation and olefin concentration and more dependent on the dissociative mechanism of phosphine. Further investigations are underway to better understand the governing factors of N_{sc} and catalyst on depolymerization behavior.

Macromolecular Metamorphosis. The concept of macromolecular metamorphosis was recently introduced by Sumerlin and co-workers, and it emphasizes that the topology of a polymer system, and its potential transformation, is equally as important as macromolecular size when designing smart materials.[53] BBs have gained notoriety for the fact that their specific architecture leads to unique properties and self-assemblies.[54−60] The densely grafted side chains occupy the pervaded volume near the backbone causing it to extend into worm-like architectures with significantly decreased entanglements. Therefore, the ability for a single material to transform from a BB architecture into a linear or different advanced architecture is predicted to introduce an entirely new class of stimuli-responsive materials.

The polypentenamer based BBs and their transformation to linear CP-PS, as described earlier, is one example of such a metamorphosis that, in theory, would allow the system to

DOI: 10.1021/jacs.9b05560
J. Am. Chem. Soc. 2019, 141, 14220−14229

become more robust as the molecules get smaller (i.e., viscosity increases after depolymerization due to the onset of more entanglements by the linear grafts). However, we also envisioned that judicious design might elevate such behavior to other transformative possibilities. In our recent report, we described the ability to produce bottlebrushes with side chains consisting of linear diblock copolymers of PS and poly(methyl methacrylate) (PMMA).[46] The core−shell bottlebrush block copolymer (BBCP), P(CPBIB$_{82}$-*g*-[S$_{21}$-*b*-MMA$_{100}$]), which has a total M_n = 1220 kg mol^{-1} and $Đ$ = 1.33, was quantitatively depolymerized using the G2 catalyst within 1 h at 80 °C ([olefin]$_0$ = 1 mM in toluene, [G2]$_0$ = 10 mol %) even with extremely large side chains. Figure 5a shows the SEC results of the BBCP (black solid trace) and the crude product after depolymerization (red dashed trace). Two peaks at lower elution times appear after depolymerization. The major peak at shorter elution time is the CP-(PS-*b*-PMMA) linear diblock copolymer (M_n = 35.2 kg mol^{-1} and $Đ$ = 1.15) while the minor peak at longer elution time is consistent with CP-PS (M_n = 3.5 kg mol^{-1} and $Đ$ = 1.10). To confirm this, the crude material was Soxhlet extracted with *n*-heptane to remove the CP-PS homopolymer leaving only the CP(PS-*b*-PMMA) (blue dashed trace, Figure 5a). Such transformations were also confirmed by ^{1}H NMR (Figures S36 and S37). Therefore, the depolymerization of these BBCPs also provides direct insight into the efficiency of ATRP to initiate and grow the PMMA from the PS grafts. It reveals that not all grafts were initiated and, more importantly, that the existing PMMA segments were three times longer ($N_{sc,MMA}$ = 293, Figure S36) than originally determined by characterization of the BBCP via ^{1}H NMR ($N_{sc,PMMA}$ = 100 which required the assumption that all PS chains were initiated).[46] Complications with ATRP of PMMA using a PS macroinitiator is to be expected due to the lower reactivity of styrenes versus methacrylates.[61] Halogen exchange is a technique likely to improve the grafting efficiency for this system going forward,[61−63] and the full depolymerization of the BBCPs will help to quantify these improvements. Nevertheless, this experiment confirms that transformation from BBCP to linear diblock copolymers is another possible metamorphosis for this system and opens the door for future investigations of solution or potentially bulk reassembly from BBCP to BCP architecture.

Another unique feature of the depolymerization process is the formation of an α-cyclopentenyl end group on each graft that can serve as a reactive site for further transformations. To illustrate this, CP-PS$_{21}$, the product of depolymerized P(CPBIB$_{181}$-*g*-S$_{18}$) in Table 1, was reacted with trimethylolpropane tris(3-mercaptopropionate) (TMP), a readily available trithiol used for thiol−ene coupling with olefins (Figure 5b). The thiol−ene reaction was promoted by the use of a photoinitiator, 2,2-dimethoxy-2-phenylacetophenone (DMPA), under UV light (Supporting Information). The transformation from CP-PS$_{21}$ (red trace) to TMP-(PS$_{21}$)$_3$ (green trace) is shown by SEC analysis in Figure 5b and ^{1}H NMR analysis in Figure S42. DSC analysis of the product shows a slight increase in T_g from 77 to 82 °C for CP-PS$_{21}$ to TMP-(PS$_{21}$)$_3$, respectively (Figures S24 and S45). Here we note CP-PS$_{21}$ coupling under these conditions was not quantitative and residual grafts were removed by extraction prior to SEC shown in Figure 5b. Nevertheless, this exciting result displays proof-of-concept where further development to increase the efficiency of the thiol−ene reaction will allow facile transformation from graft to star architectures.

Figure 5c shows a totality of macromolecular metamorphosis possible and reported in this work through various stages starting from the original linear polypentenamer, to BB, to linear graft, and finally to 3-arm stars. Representative SEC traces for each transformation are also shown. Seemingly limitless possibilities for new stimuli-responsive materials are predicted as the chemistries and architectures of the grafts on a polypentenamer backbone are diversified.

CONCLUSIONS

The depolymerization of polypentenamer BBs was investigated for the first time. SEC data suggests that depolymerization occurs through an end-to-end mechanism starting from the terminal olefin and subsequent RCM to fully deconstruct the backbone. This is in direct contrast to linear PCPs that are shown to depolymerize in a random fashion. Quantitative depolymerization of the BBs can be performed at varying N_{sc} and N_{bb} using widely available Ru catalysts. Catalyst screening showed that G2 and G3 depolymerized the BBs up to 300 times faster than HG2 under similar conditions. The decreased depolymerization rate of HG2 is potentially a result of the boomerang mechanism, which also supports the claim that depolymerization begins on the terminal olefin end of the BB. The N_{bb} and N_{sc} of the BB had little effect on the depolymerization kinetics, requiring continued investigations regarding the rate orders that govern this process. Diblock copolymer side chains as long as 40 kg mol^{-1} were found to still enable quantitative depolymerization of the PCP backbone of BBCPs. Deconstruction of the BB architecture provides opportunities for macromolecular metamorphosis into linear homopolymers, block polymers, and a seemingly limitless selection of other graft designs not yet explored. The α-cyclopentenyl end group produced on each graft following BB depolymerization also serves as a reactive site to enable the transformation to other architectures, such as 3-arm star polymers. Further studies are ongoing to fully elucidate the governing factors and mechanistic details of the proposed end-to-end depolymerization mechanism.

ASSOCIATED CONTENT

Supporting Information

The Supporting Information is available free of charge on the ACS Publications website at DOI: 10.1021/jacs.9b05560.

Materials, methods, and further characterization data (PDF)

AUTHOR INFORMATION

Corresponding Author

*kennemur@chem.fsu.edu (J.G.K.)

ORCID

Justin G. Kennemur: 0000-0002-2322-0386

Notes

The authors declare no competing financial interest.

ACKNOWLEDGMENTS

This work was supported by the National Science Foundation under Grant No. 1750852. J.G.K wishes to thank Brent Sumerlin, Javid Rzayev, and Luis Campos for helpful discussions and Umicore for generous donation of Ru catalysts M1a (G1), M2a (G2), and M72 (HG2). ^{1}H and ^{13}C NMR were performed in the FSU Department of Chemistry and

DOI: 10.1021/jacs.9b05560
J. Am. Chem. Soc. 2019, 141, 14220−14229

Biochemistry NMR Facility under the supervision of Dr. Banghao Chen. We also thank Prof. Albert Steigman for use of the DSC instrument.

REFERENCES

(1) Sagi, A.; Weinstain, R.; Karton, N.; Shabat, D. Self-Immolative Polymers. *J. Am. Chem. Soc.* **2008**, *130*, 5434−5435.
(2) Wang, W.; Alexander, C. Self-Immolative Polymers. *Angew. Chem., Int. Ed.* **2008**, *47*, 7804−7806.
(3) Peterson, G. I.; Larsen, M. B.; Boydston, A. J. Controlled Depolymerization: Stimuli-Responsive Self-Immolative Polymers. *Macromolecules* **2012**, *45*, 7317−7328.
(4) Phillips, S. T.; DiLauro, A. M. Continuous Head-to-Tail Depolymerization: An Emerging Concept for Imparting Amplified Responses to Stimuli-Responsive Materials. *ACS Macro Lett.* **2014**, *3*, 298−304.
(5) Roth, M. E.; Green, O.; Gnaim, S.; Shabat, D. Dendritic, Oligomeric, and Polymeric Self-Immolative Molecular Amplification. *Chem. Rev.* **2016**, *116*, 1309−1352.
(6) Stuart, M. A. C.; Huck, W. T. S.; Genzer, J.; Müller, M.; Ober, C.; Stamm, M.; Sukhorukov, G. B.; Szleifer, I.; Tsukruk, V. V.; Urban, M.; Winnik, F.; Zauscher, S.; Luzinov, I.; Minko, S. Emerging applications of stimuli-responsive polymer materials. *Nat. Mater.* **2010**, *9*, 101.
(7) Weinstain, R.; Sagi, A.; Karton, N.; Shabat, D. Self-Immolative Comb-Polymers: Multiple-Release of Side-Reporters by a Single Stimulus Event. *Chem. - Eur. J.* **2008**, *14*, 6857−6861.
(8) Yeung, K.; Kim, H.; Mohapatra, H.; Phillips, S. T. Surface-Accessible Detection Units in Self-Immolative Polymers Enable Translation of Selective Molecular Detection Events into Amplified Responses in Macroscopic, Solid-State Plastics. *J. Am. Chem. Soc.* **2015**, *137*, 5324−5327.
(9) Miller, K. A.; Morado, E. G.; Samanta, S. R.; Walker, B. A.; Nelson, A. Z.; Sen, S.; Tran, D. T.; Whitaker, D. J.; Ewoldt, R. H.; Braun, P. V.; Zimmerman, S. C. Acid-Triggered, Acid-Generating, and Self-Amplifying Degradable Polymers. *J. Am. Chem. Soc.* **2019**, *141*, 2838−2842.
(10) Esser-Kahn, A. P.; Sottos, N. R.; White, S. R.; Moore, J. S. Programmable Microcapsules from Self-Immolative Polymers. *J. Am. Chem. Soc.* **2010**, *132*, 10266−10268.
(11) Esser-Kahn, A. P.; Odom, S. A.; Sottos, N. R.; White, S. R.; Moore, J. S. Triggered Release from Polymer Capsules. *Macromolecules* **2011**, *44*, 5539−5553.
(12) Wong, A. D.; DeWit, M. A.; Gillies, E. R. Amplified release through the stimulus triggered degradation of self-immolative oligomers, dendrimers, and linear polymers. *Adv. Drug Delivery Rev.* **2012**, *64*, 1031−1045.
(13) Liu, G.; Wang, X.; Hu, J.; Zhang, G.; Liu, S. Self-Immolative Polymersomes for High-Efficiency Triggered Release and Programmed Enzymatic Reactions. *J. Am. Chem. Soc.* **2014**, *136*, 7492−7497.
(14) Liu, G.; Zhang, G.; Hu, J.; Wang, X.; Zhu, M.; Liu, S. Hyperbranched Self-Immolative Polymers (hSIPs) for Programmed Payload Delivery and Ultrasensitive Detection. *J. Am. Chem. Soc.* **2015**, *137*, 11645−11655.
(15) Fan, B.; Gillies, E. R. Poly(ethyl glyoxylate)-Poly(ethylene oxide) Nanoparticles: Stimuli-Responsive Drug Release via End-to-End Polyglyoxylate Depolymerization. *Mol. Pharmaceutics* **2017**, *14*, 2548−2559.
(16) Wang, Z.; Wu, H.; Liu, P.; Zeng, F.; Wu, S. A self-immolative prodrug nanosystem capable of releasing a drug and a NIR reporter for in vivo imaging and therapy. *Biomaterials* **2017**, *139*, 139−150.
(17) Xie, Y.; Murray-Stewart, T.; Wang, Y.; Yu, F.; Li, J.; Marton, L. J.; Casero, R. A.; Oupický, D. Self-immolative nanoparticles for simultaneous delivery of microRNA and targeting of polyamine metabolism in combination cancer therapy. *J. Controlled Release* **2017**, *246*, 110−119.
(18) Weinstain, R.; Baran, P. S.; Shabat, D. Activity-Linked Labeling of Enzymes by Self-Immolative Polymers. *Bioconjugate Chem.* **2009**, *20*, 1783−1791.
(19) Ergene, C.; Palermo, E. F. Cationic Poly(benzyl ether)s as Self-Immolative Antimicrobial Polymers. *Biomacromolecules* **2017**, *18*, 3400−3409.
(20) Ergene, C.; Palermo, E. F. Self-immolative polymers with potent and selective antibacterial activity by hydrophilic side chain grafting. *J. Mater. Chem. B* **2018**, *6*, 7217−7229.
(21) Zhang, H.; Yeung, K.; Robbins, J. S.; Pavlick, R. A.; Wu, M.; Liu, R.; Sen, A.; Phillips, S. T. Self-Powered Microscale Pumps Based on Analyte-Initiated Depolymerization Reactions. *Angew. Chem., Int. Ed.* **2012**, *51*, 2400−2404.
(22) Baker, M. S.; Kim, H.; Olah, M. G.; Lewis, G. G.; Phillips, S. T. Depolymerizable poly(benzyl ether)-based materials for selective room temperature recycling. *Green Chem.* **2015**, *17*, 4541−4545.
(23) Chen, E. K. Y.; McBride, R. A.; Gillies, E. R. Self-Immolative Polymers Containing Rapidly Cyclizing Spacers: Toward Rapid Depolymerization Rates. *Macromolecules* **2012**, *45*, 7364−7374.
(24) de Gracia Lux, C.; McFearin, C. L.; Joshi-Barr, S.; Sankaranarayanan, J.; Fomina, N.; Almutairi, A. Single UV or Near IR Triggering Event Leads to Polymer Degradation into Small Molecules. *ACS Macro Lett.* **2012**, *1*, 922−926.
(25) DeWit, M. A.; Gillies, E. R. A Cascade Biodegradable Polymer Based on Alternating Cyclization and Elimination Reactions. *J. Am. Chem. Soc.* **2009**, *131*, 18327−18334.
(26) Fan, B.; Trant, J. F.; Hemery, G.; Sandre, O.; Gillies, E. R. Thermo-responsive self-immolative nanoassemblies: direct and indirect triggering. *Chem. Commun.* **2017**, *53*, 12068−12071.
(27) Fan, B.; Trant, J. F.; Wong, A. D.; Gillies, E. R. Polyglyoxylates: A Versatile Class of Triggerable Self-Immolative Polymers from Readily Accessible Monomers. *J. Am. Chem. Soc.* **2014**, *136*, 10116−10123.
(28) Gambles, M. T.; Fan, B.; Borecki, A.; Gillies, E. R. Hybrid Polyester Self-Immolative Polymer Nanoparticles for Controlled Drug Release. *ACS Omega* **2018**, *3*, 5002−5011.
(29) Olah, M. G.; Robbins, J. S.; Baker, M. S.; Phillips, S. T. End-Capped Poly(benzyl ethers): Acid and Base Stable Polymers That Depolymerize Rapidly from Head-to-Tail in Response to Specific Applied Signals. *Macromolecules* **2013**, *46*, 5924−5928.
(30) Peterson, G. I.; Church, D. C.; Yakelis, N. A.; Boydston, A. J. 1,2-oxazine linker as a thermal trigger for self-immolative polymers. *Polymer* **2014**, *55*, 5980−5985.
(31) Seo, W.; Phillips, S. T. Patterned Plastics That Change Physical Structure in Response to Applied Chemical Signals. *J. Am. Chem. Soc.* **2010**, *132*, 9234−9235.
(32) Sirianni, Q. E. A.; Rabiee Kenaree, A.; Gillies, E. R. Polyglyoxylamides: Tuning Structure and Properties of Self-Immolative Polymers. *Macromolecules* **2019**, *52*, 262−270.
(33) Kaitz, J. A.; Possanza, C. M.; Song, Y.; Diesendruck, C. E.; Spiering, A. J. H.; Meijer, E. W.; Moore, J. S. Depolymerizable, adaptive supramolecular polymer nanoparticles and networks. *Polym. Chem.* **2014**, *5*, 3788−3794.
(34) Olejniczak, J.; Nguyen Huu, V. A.; Lux, J.; Grossman, M.; He, S.; Almutairi, A. Light-triggered chemical amplification to accelerate degradation and release from polymeric particles. *Chem. Commun.* **2015**, *51*, 16980−16983.
(35) Diesendruck, C. E.; Peterson, G. I.; Kulik, H. J.; Kaitz, J. A.; Mar, B. D.; May, P. A.; White, S. R.; Martínez, T. J.; Boydston, A. J.; Moore, J. S. Mechanically triggered heterolytic unzipping of a low-ceiling-temperature polymer. *Nat. Chem.* **2014**, *6*, 623.
(36) Zhang, Y.; Ma, L.; Deng, X.; Cheng, J. Trigger-responsive chain-shattering polymers. *Polym. Chem.* **2013**, *4*, 224−228.
(37) DiLauro, A. M.; Lewis, G. G.; Phillips, S. T. Self-Immolative Poly(4,5-dichlorophthalaldehyde) and its Applications in Multi-Stimuli-Responsive Macroscopic Plastics. *Angew. Chem., Int. Ed.* **2015**, *54*, 6200−6205.

DOI: 10.1021/jacs.9b05560
J. Am. Chem. Soc. 2019, 141, 14220−14229

(38) Xiao, Y.; Li, Y.; Zhang, B.; Li, H.; Cheng, Z.; Shi, J.; Xiong, J.; Bai, Y.; Zhang, K. Functionalizable, Side Chain-Immolative Poly(benzyl ether)s. *ACS Macro Lett.* **2019**, *8*, 399−402.
(39) Xiao, Y.; Li, H.; Zhang, B.; Cheng, Z.; Li, Y.; Tan, X.; Zhang, K. Modulating the Depolymerization of Self-Immolative Brush Polymers with Poly(benzyl ether) Backbones. *Macromolecules* **2018**, *51*, 2899−2905.
(40) Neary, W. J.; Kennemur, J. G. Polypentenamer Renaissance: Challenges and Opportunities. *ACS Macro Lett.* **2019**, *8*, 46−56.
(41) Ofstead, E. A.; Calderon, N. Equilibrium ring-opening polymerization of mono- and multicyclic unsaturated monomers. *Makromol. Chem.* **1972**, *154*, 21−34.
(42) Tuba, R.; Balogh, J.; Hlil, A.; Barłóg, M.; Al-Hashimi, M.; Bazzi, H. S. Synthesis of Recyclable Tire Additives via Equilibrium Ring-Opening Metathesis Polymerization. *ACS Sustainable Chem. Eng.* **2016**, *4*, 6090−6094. (Note: An error within the main manuscript of this reference suggests that G2 was used for depolymerization, but the SI document accurately describes HG2 as the catalyst used. We thank R. Tuba for this clarification.)
(43) Liu, H.; Nelson, A. Z.; Ren, Y.; Yang, K.; Ewoldt, R. H.; Moore, J. S. Dynamic Remodeling of Covalent Networks via Ring-Opening Metathesis Polymerization. *ACS Macro Lett.* **2018**, *7*, 933−937.
(44) Badamshina, E. R.; Korshak, Y. V.; Berlin, A. A.; Vdovin, V. M.; Kutepov, D. F.; Pavlova, S. A.; Timofeyeva, G. I. Investigation of the Mechanism of Polypentenamer Degradation in the Prescence of Metathesis Catalysts. *Polym. Sci. USSR* **1982**, *24*, 164−170.
(45) Neary, W. J.; Kennemur, J. G. Variable Temperature ROMP: Leveraging Low Ring Strain Thermodynamics To Achieve Well-Defined Polypentenamers. *Macromolecules* **2017**, *50*, 4935−4941.
(46) Neary, W. J.; Fultz, B. A.; Kennemur, J. G. Well-Defined and Precision-Grafted Bottlebrush Polypentenamers from Variable Temperature ROMP and ATRP. *ACS Macro Lett.* **2018**, *7*, 1080−1086.
(47) Mulhearn, W. D.; Register, R. A. Synthesis of Narrow-Distribution, High-Molecular-Weight ROMP Polycyclopentene via Suppression of Acyclic Metathesis Side Reactions. *ACS Macro Lett.* **2017**, *6*, 112−116.
(48) Matyjaszewski, K. Atom Transfer Radical Polymerization (ATRP): Current Status and Future Perspectives. *Macromolecules* **2012**, *45*, 4015−4039.
(49) Cheng, C.; Khoshdel, E.; Wooley, K. L. Facile One-Pot Synthesis of Brush Polymers through Tandem Catalysis Using Grubbs' Catalyst for Both Ring-Opening Metathesis and Atom Transfer Radical Polymerizations. *Nano Lett.* **2006**, *6*, 1741−1746.
(50) Tuba, R.; Grubbs, R. H. Ruthenium catalyzed equilibrium ring-opening metathesis polymerization of cyclopentene. *Polym. Chem.* **2013**, *4*, 3959−3962.
(51) Bates, J. M.; Lummiss, J. A. M.; Bailey, G. A.; Fogg, D. E. Operation of the Boomerang Mechanism in Olefin Metathesis Reactions Promoted by the Second-Generation Hoveyda Catalyst. *ACS Catal.* **2014**, *4*, 2387−2394.
(52) Sanford, M. S.; Ulman, M.; Grubbs, R. H. New Insights into the Mechanism of Ruthenium-Catalyzed Olefin Metathesis Reactions. *J. Am. Chem. Soc.* **2001**, *123*, 749−750.
(53) Sun, H.; Kabb, C. P.; Dai, Y.; Hill, M. R.; Ghiviriga, I.; Bapat, A. P.; Sumerlin, B. S. Macromolecular metamorphosis via stimulus-induced transformations of polymer architecture. *Nat. Chem.* **2017**, *9*, 817.
(54) Feng, C.; Li, Y.; Yang, D.; Hu, J.; Zhang, X.; Huang, X. Well-defined graft copolymers: from controlled synthesis to multipurpose applications. *Chem. Soc. Rev.* **2011**, *40*, 1282−1295.
(55) Liberman-Martin, A. L.; Chu, C. K.; Grubbs, R. H. Application of Bottlebrush Block Copolymers as Photonic Crystals. *Macromol. Rapid Commun.* **2017**, *38*, 1700058.
(56) Müllner, M.; Müller, A. H. E. Cylindrical polymer brushes − Anisotropic building blocks, unimolecular templates and particulate nanocarriers. *Polymer* **2016**, *98*, 389−401.
(57) Rzayev, J. Molecular Bottlebrushes: New Opportunities in Nanomaterials Fabrication. *ACS Macro Lett.* **2012**, *1*, 1146−1149.
(58) Sheiko, S. S.; Sumerlin, B. S.; Matyjaszewski, K. Cylindrical molecular brushes: Synthesis, characterization, and properties. *Prog. Polym. Sci.* **2008**, *33*, 759−785.
(59) Verduzco, R.; Li, X.; Pesek, S. L.; Stein, G. E. Structure, function, self-assembly, and applications of bottlebrush copolymers. *Chem. Soc. Rev.* **2015**, *44*, 2405−2420.
(60) Xie, G.; Martinez, M. R.; Olszewski, M.; Sheiko, S. S.; Matyjaszewski, K. Molecular Bottlebrushes as Novel Materials. *Biomacromolecules* **2019**, *20*, 27−54.
(61) Braunecker, W. A.; Matyjaszewski, K. Controlled/living radical polymerization: Features, developments, and perspectives. *Prog. Polym. Sci.* **2007**, *32*, 93−146.
(62) Peng, C.-H.; Kong, J.; Seeliger, F.; Matyjaszewski, K. Mechanism of Halogen Exchange in ATRP. *Macromolecules* **2011**, *44*, 7546−7557.
(63) Shipp, D. A.; Wang, J.-L.; Matyjaszewski, K. Synthesis of Acrylate and Methacrylate Block Copolymers Using Atom Transfer Radical Polymerization. *Macromolecules* **1998**, *31*, 8005−8008.

DOI: 10.1021/jacs.9b05560
J. Am. Chem. Soc. 2019, 141, 14220−14229